

Magnetic ground state and excitations in mixed 3d-4d quasi-1D spin-chain oxide $\text{Sr}_3\text{NiRhO}_6$

A. Jain,^{1,2,*} D. T. Adroja,^{3,4,†} S. Rayaprol,⁵ A. D. Hillier,³
W. Kockelmann,³ S. M. Yusuf,^{1,2} and E. V. Sampathkumaran^{6,7}

¹*Solid State Physics Division, Bhabha Atomic Research Centre, Mumbai 400085, India*

²*Homi Bhabha National Institute, Anushaktinagar, Mumbai 400 094, India*

³*ISIS Facility, STFC, Rutherford Appleton Laboratory, Chilton, Oxfordshire OX11 0QX, UK*

⁴*Highly Correlated Matter Research Group, Physics Department,*

University of Johannesburg, PO Box 524, Auckland Park 2006, South Africa

⁵*UGC-DAE CSR, Mumbai Center, CFB, BARC, Trombay, Mumbai 400085, India*

⁶*Department of Physics, Indian Institute of Technology Roorkee, Roorkee 247667, India*

⁷*Tata Institute of Fundamental Research, Homi Bhabha Road, Colaba, Mumbai 400005, India*

(Dated: November 20, 2024)

Entanglement of spin and orbital degrees of freedom, via relativistic spin-orbit coupling, in 4d transition metal oxides can give rise to a variety of novel quantum phases. A previous study of mixed 3d-4d quasi-1D spin-chain oxide $\text{Sr}_3\text{NiRhO}_6$ using the magnetization measurements by Mohapatra *et al.* [Phys. Rev. B 75, 214422 (2007)] revealed a partially disordered antiferromagnetic (PDA) structure below 50 K [1]. We here report the magnetic ground state and spin-wave excitations in $\text{Sr}_3\text{NiRhO}_6$ using muon spin rotation and relaxation (μSR), and neutron (elastic and inelastic) scattering techniques. Our neutron diffraction study reveals that in the magnetic structure of $\text{Sr}_3\text{NiRhO}_6$ Rh⁴⁺ and Ni²⁺ spins are aligned ferromagnetically in a spin-chain, with moments along the crystallographic *c*-axis. However, spin-chains are coupled antiferromagnetically in the *ab*-plane. μSR reveals the presence of oscillations in the asymmetry-time spectra below 50 K, supporting the long-range magnetically ordered ground state. Our inelastic neutron scattering study reveals gapped quasi-1D magnetic excitations with a large ratio of gap to exchange interaction. The observed spin-wave spectrum could be well fitted with a ferromagnetic isotropic exchange model (with $J = 3.7$ meV) and single ion anisotropy ($D = 10$ meV) on the Ni²⁺ site. The magnetic excitations survive up to 85 K, well above the magnetic ordering temperature of ~ 50 K, also indicating a quasi-1D nature of the magnetic interactions in $\text{Sr}_3\text{NiRhO}_6$.

PACS numbers: 75.25.-j, 75.30.Cr, 75.30.Ds, 75.30.Gw, 75.40.Gb, 75.40.Mg, 75.47.Lx

I. INTRODUCTION

Quasi-one-dimensional (1D) quantum spin-chain compounds have attracted a lot of attention in the last two decades due to a variety of interesting quantum phenomenon revealed by them. Among these, spin-chain compounds with general formula A_3MXO_6 (A here denote Sr, Ca, etc. and M , X denote transition metals) have attracted much attention in recent years [1–40], due to their peculiar properties such as time dependent magnetic order [24, 40], steps in the dc magnetization [13], order by disorder [21], and multiferroicity [19]. The crystal structures of these compounds contain spin-chains, made up of alternating face-sharing XO_6 octahedra (OCT) and MO_6 trigonal prisms (TP), running along the crystallographic *c*-axis (Fig. 1) [2]. These chains are arranged on a triangular lattice in the *ab*-plane. In most of the compounds, where 3d transition metal ions occupy both OCT and TP sites, intrachain magnetic exchange interaction is ferromagnetic (FM) [28, 37]. This combined

with an antiferromagnetic (AFM) interchain interaction and triangular lattice arrangement of spin-chains gives rise to geometrically frustrated magnetism [12, 17, 18, 28, 35, 37]. Among these compounds, the cobalt base system $\text{Ca}_3\text{Co}_2\text{O}_6$ has been extensively investigated in last two decades [5, 10–12, 14, 17, 18, 25, 28, 31, 35, 37, 40]. Due to spin-orbit coupling (~ 70 meV) cobalt ions in $\text{Ca}_3\text{Co}_2\text{O}_6$ show Ising-like behaviour, with spin aligned ferromagnetically along the crystallographic *c*-axis.

Initial interest in the compounds, where 3d transition metal ions occupy both OCT and TP sites, was motivated because correlation effects are more prominent in 3d transition metal than for the 4d and 5d transition metal ions. However, discovery of a Mott insulating state in Sr_2IrO_4 in the late 2000s [41] and the role of spin-orbit coupling (SOC) in stabilizing the Mott state awoke an interest in the compounds where spin-chains were made up of 3d and 5d spin-chain oxides. Subsequently, many Sr-based compounds of the A_3MXO_6 family, namely Sr_3MIrO_6 with $M=\text{Co}$, Cu , Ni , and Zn , were in-

vestigated [4, 6, 7, 9, 22, 27, 33, 34, 38, 39]. For $\text{Sr}_3\text{CuIrO}_6$ [30], a large gap in the magnetic excitation spectrum was observed which was ascribed to an unusual exchange anisotropy generating mechanism, namely, strong FM anisotropy arising from AFM super-exchange interaction, driven by the alternating weak and strong spin-orbit coupling on the $3d$ Cu and $5d$ Ir magnetic ions, respectively. Non-collinear AFM ordering has been observed in $\text{Sr}_3\text{ZnIrO}_6$ and $\text{Sr}_3\text{ZnRhO}_6$ which has been ascribed to anisotropic intra-chain and inter-chain exchange interactions [23, 39], arising due to a strong spin-orbit coupling. In $\text{Sr}_3\text{NiRhO}_6$, anisotropic symmetric interaction from strong spin-orbit coupling was theoretically proposed to result in a strong magnetic anisotropy and AFM intrachain interactions [42]. Therefore, in search of unusual magnetic behavior expected in the mixed $3d$ and $4d$ transition-metal compounds via exchange pathways that are absent in the compound with only $3d$ transition-metal ions, some of us reported interesting magnetic anomalies with partially disordered antiferromagnetism in $\text{Sr}_3\text{NiRhO}_6$, based on bulk magnetization techniques [1]. This kind of magnetism has garnered significant interest in recent years, as the magnetic ions of a given element occupy crystallographically equivalent positions, but only some of these ions exhibit magnetic ordering while others remain magnetically disordered due to geometrical frustration. Unlike spin liquids, where disorder is uniform and intrinsic, partially disordered magnets feature order and disorder coexisting in the same magnetic phase, resulting in unique physical properties and potential applications.

We here present the results of an extensive investigation of the magnetism of $\text{Sr}_3\text{NiRhO}_6$ using muon spin rotation and relaxation (μSR), elastic and inelastic neutron scattering techniques, to gain a deeper microscopic insight into the nature of geometrically frustrated magnetism in this compound. The present study firmly establishes that this compound orders in a partially disordered antiferromagnetic (PDA) state below ~ 50 K (T_1). The PDA state undergoes a transition to a frozen PDA (FPDA) below ~ 20 K (T_2). Further, our inelastic neutron scattering study confirms the 1D nature of the magnetism of this compound.

II. EXPERIMENTAL DETAILS

Polycrystalline samples were synthesized by the standard solid state reaction method starting with high purity materials SrCO_3 (99.99%), NiO

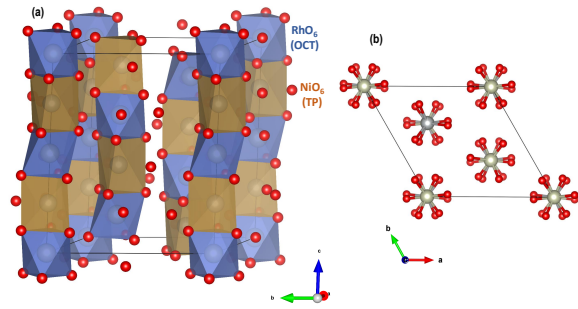


FIG. 1. (Color online) Crystal structure of $\text{Sr}_3\text{NiRhO}_6$: A perspective view showing 1D spin-chains made up of alternating face-sharing NiO_6 trigonal prisms and RhO_6 octahedra (left). Right side shows triangular lattice arrangement of spin-chain in ab -plane. Red balls show O atoms. For clarity strontium atoms are not shown.

(99.99%), and RhO_2 (99.9%) in powder form, as discussed in ref. [1]. The magnetization measurements (dc and ac) were carried out using a Quantum Design SQUID VSM to confirm the quality of the specimen magnetically vis-a-vis the ones reported in Ref. [1] [See Appendices A and B]. The neutron diffraction experiments at 297 K were carried out using the five linear position sensitive detector (PSD) based powder diffractometer ($\lambda = 1.249\text{\AA}$) at Dhruva research reactor, Trombay. Neutron diffraction experiments in the temperature range 5-100 K were performed using the time-of-flight GEM diffractometer at the ISIS facility, UK. The diffraction data were analyzed by the Rietveld method, using the FULLPROF program [43]. The inelastic neutron scattering (INS) measurements over 5-300 K were performed using the time-of-flight chopper spectrometer HET at the ISIS Neutron and Muon Facility, UK. Muon Spin Rotation and Relaxation (μSR) experiments were carried out using the MuSR spectrometer at the ISIS Neutron and Muon Facility, UK.

III. RESULTS

A. Crystal Structure: Neutron Diffraction

Figure 2 depicts the Rietveld refined neutron diffraction pattern at 297 K for $\text{Sr}_3\text{NiRhO}_6$ measured at Dhruva research reactor using a wavelength of 1.249\AA . The refined values of the lattice constants $a = 9.585(1)$, and $c = 11.041(1)\text{\AA}$ (space group $R\bar{3}c$) are found to be in good agreement with those reported in the literature [1, 44, 45]. There

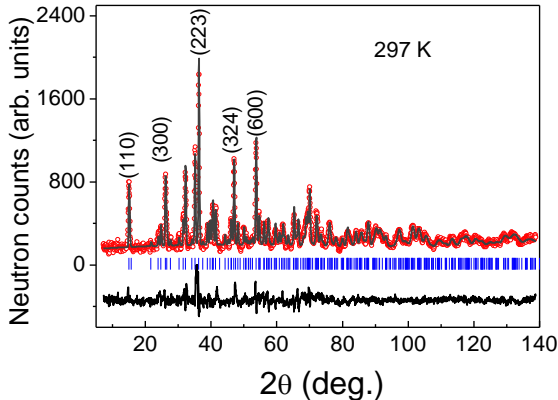


FIG. 2. (Color online) Observed (data points) and calculated (solid line through the data points) neutron diffraction patterns for $\text{Sr}_3\text{NiRhO}_6$ at 297 K using a wavelength of 1.249 \AA . The black solid line at the bottom shows the difference between the observed and the calculated patterns. Vertical lines show the positions of the nuclear Bragg peaks. The (hkl) values corresponding to a few strong Bragg peaks are also listed.

are six formula units ($Z = 6$) of $\text{Sr}_3\text{NiRhO}_6$ in a crystallographic unit cell. The refinement also confirms that Ni^{2+} and Rh^{4+} ions are located at the TP and OCT sites, respectively. We have also performed a detailed analysis of neutron diffraction pattern at 100 K, collected using the time-of-flight GEM diffractometer at the ISIS facility, UK, covering a wide Q -range (Fig. 13, Appendix C). The unit cell parameters and other structural parameters obtained from the refinement of the neutron diffraction patterns at 100 K are given in Table I.

B. Magnetic Structure: Neutron Diffraction

To investigate the magnetic ground state of $\text{Sr}_3\text{NiRhO}_6$, we have performed neutron diffraction experiments over 5-100 K. Fig. 3(a-b) shows Rietveld refined neutron diffraction patterns obtained from the GEM instrument at 5 and 100 K. The neutron diffraction patterns at 100 K can be fitted by considering only the nuclear phase. The nuclear peaks as inferred from 100 K data are shown in (Fig. 3(a)) to compare with the pattern shown in (Fig. 3(b)). As shown in Fig. 3(b), an additional peak in the neutron diffraction pattern is clearly visible at $Q \sim 0.76 \text{ \AA}^{-1}$ at 5 K compared with the 100 K data. The temperature dependence of the integrated intensity of the additional Bragg peak is shown in the inset of Fig. 3(a). The difference pattern between 5 and 100 K [Figs. 3(c-

d)], obtained from the detector bank-2 and bank-3, highlights distinct magnetic Bragg peaks, indicating long-range magnetic ordering. The propagation vector for the observed magnetic peaks is $k = (0, 0, 1)$ in the hexagonal setting of the space group $R\bar{3}c$. In the primitive rhombohedral cell setting, Kovalev's notation, $k = (1/3, 1/3, 1/3)$. Analysis of magnetic structure has been carried out using the standard irreducible representation theory with help of software BASIREPS [43]. In $\text{Sr}_3\text{NiRhO}_6$, Rh^{4+} and Ni^{2+} ions are located at the $6b$ $(0, 0, 0)$ and $6a$ $(0, 0, 1/4)$ sites, respectively. The magnetic reducible representations for these sites can be decomposed as direct sum of irreducible representations as

$$\Gamma(6b) = 1\Gamma_1^{(1)} + 1\Gamma_2^{(1)} + 2\Gamma_3^{(2)} \quad (1)$$

and

$$\Gamma(6a) = 1\Gamma_1^{(1)} + 1\Gamma_2^{(1)} + 2\Gamma_3^{(2)}. \quad (2)$$

The representations Γ_1 and Γ_2 are one-dimensional, while representation Γ_3 is two dimensional. In the formalism of propagation vectors, the magnetic moment of the atom “ j ” in the asymmetric magnetic unit cell with the origin at the lattice point R_L , can be written as the Fourier series of the form

$$\mathbf{m}_{L,j} = \sum_{\mathbf{k}} \mathbf{S}_j^{\mathbf{k}} \exp(-2\pi i \mathbf{k} \cdot \mathbf{R}_L). \quad (3)$$

These Fourier coefficients, $\mathbf{S}_j^{\mathbf{k}}$, can be written as a linear combination of the basis vectors of the irreducible representation of the propagation vector group \mathbf{G}_k . In the Bertaut method [46], the magnetic structure is derived by coupling the basis vectors corresponding to the same representation at different sites. Therefore, we first consider the representations Γ_1 and Γ_2 to describe the magnetic structure. The basis vectors for Γ_1 and Γ_2 representations are shown in Table II. In the Γ_1 representation, spins along the c -axis are antiferromagnetically coupled, while in the Γ_2 spins along the c -axis are ferromagnetically coupled. The observed magnetic structure of the present compound can be fitted using the representation Γ_2 . In the magnetic structure magnetic moments, in a spin-chain, are aligned ferromagnetically along the crystallographic c axis, however, spin-chains are coupled antiferromagnetically in the ab -plane with net zero moment in the unit cell. The refined values of ordered magnetic moment for $6a$ (Ni^{2+}) and $6b$ (Rh^{4+}) sites are 0.88 (1) and 0.12 (1) μ_B , respectively. The observed value of magnetic moment is

TABLE I. Structural parameters (atomic positions, thermal parameters, obtained from the refinement of the neutron diffraction patterns at 100 K for $\text{Sr}_3\text{NiRhO}_6$. The lattice constants are $a = 9.569(1)$ Å, $c = 11.025(2)$ Å. All crystallographic sites are fully occupied.

Atom	Site	x	y	z	$B_{iso}(\text{Å}^2)$
Sr	18e	0.3661(5)	0	0.25	0.29(2)
Rh	6b	0	0	0	0.28 (3)
Ni	6a	0	0	0.25	0.23(3)
O	36f	0.1720(1)	0.0209(3)	0.1129(2)	0.33(3)

much smaller than theoretically expected value of 2 and $1 \mu_B$ for Ni^{2+} and Rh^{4+} , respectively (assuming $g = 2$). The observed small value of the ordered moment could be attributed to enhanced quantum fluctuations associated with geometrical frustration and the low dimensionality of the present system. The symmetry analysis mandates that an amplitude modulated structure with no vanishing moment at any site (Fig. 4(a)) differs from a partially disordered antiferromagnetic (PDA) structure (Fig. 4(b)) by a global phase that cannot be determined using powder diffraction. Nevertheless, equivalence of the two magnetic structure models was validated without relying on symmetry assumptions. Therefore, we also fitted the observed neutron diffraction pattern using the space group $P\bar{1}$, and propagation vector $k = (0, 0, 0)$ and obtained similar chi-square (χ^2) values for the amplitude modulated and PDA configurations. In the PDA state, 2/3 of ferromagnetically coupled spin-chains are ordered in the AFM structure, while the remaining 1/3 are in the incoherent state (with net zero ordered state moment). The schematics of PDA and amplitude modulated structure suitable for $\text{Sr}_3\text{NiRhO}_6$ are shown in Fig. 4. It can be noted that, based on the behavior of ac susceptibility (Appendix B) where a large shift in the peak position was observed with frequency, the magnetic ground state can be considered as F-PDA state below 20 K. In the F-PDA state, spins in the 1/3 incoherent chains of PDA state freeze randomly, indicating that magnetic ground state might not be thermodynamically stable. This F-PDA state is compatible with the PDA structure (Fig. 4(b)) from neutron diffraction.

C. Muon spin relaxation

In order to investigate the microscopic nature of magnetic order in $\text{Sr}_3\text{NiRhO}_6$ we have used the μSR technique, which is very sensitive to the local mag-

TABLE II. Basis vectors of positions 6a and 6b for the representations Γ_1 and Γ_2 .

IR	Basis vectors for 6b site	Basis vectors for 6a site
	(0, 0, 0)	(0, 0, 1/2)
	(0, 0, 1/4)	(0, 0, 3/4)
Γ_1	(0 0 1)	(0 0 -1)
Γ_2	(0 0 1)	(0 0 1)

netic moment and its environments, because the implanted muons in the sample experience magnetic field of nearest neighbors. Figure 5 shows the zero-field (ZF)- μSR spectrum of $\text{Sr}_3\text{NiRhO}_6$ at various temperatures over 1.4-100 K. In the paramagnetic regime ($T > T_1$), due to thermal fluctuations, the magnetic moments become disordered, leading to a random orientation of the spins in both time and space. As a result, the expectation value of the local magnetic field at the muon site $\langle B_\mu \rangle = 0$, which prevent coherent muon spin precession. For polycrystalline samples, this results in an exponential relaxation of the muon polarization signal. Below $T < T_1$, ZF spectra exhibit two minima (i.e. oscillation with time), indicating the onset of a long-range magnetic ordering. Our analysis shows that there are two muon sites, one site with a field greater than the frequency response of the μSR spectrometer at ISIS pulsed muon facility due to the pulsed width of 80ns. In the first approximation, the observed spectra seem to be typical for Kubo-Toyabe-type relaxation. However, a careful analysis has shown that a Gaussian damped oscillatory function (mentioned below), probably due to a static order with wide field distribution, is more suitable for fitting the μSR asymmetry spectra.

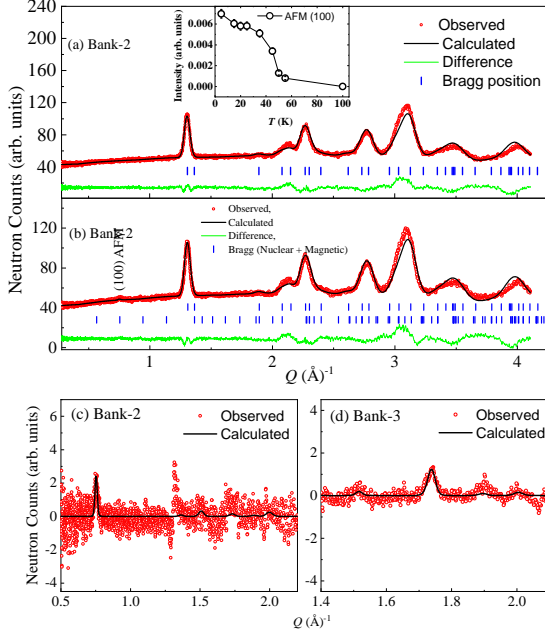


FIG. 3. (Color online) Rietveld refined neutron diffraction patterns at (a) 100 and (b) 5 K from the detector bank-2 of the GEM diffractometer. Upper (lower) vertical lines show the positions of the nuclear (magnetic) Bragg peaks. Observed (open circles) and calculated (solid line) neutron diffraction patterns. Solid green line at the bottom shows the difference between the observed and the calculated patterns. The inset in (a) shows the temperature dependent intensity of the magnetic Bragg peak. Observed (open circles) neutron powder diffraction pattern at 5 K after subtraction of the nuclear pattern at 100 K and calculated (solid lines) pattern considering only magnetic phase with zero background from the (c) detector bank-2 and (d) detector bank-3 over low values of Q from the GEM TOF diffractometer. The GEM detector banks 2 and 3 are positioned at scattering angles of 17.980° and 34.960° , respectively. Due to their distinct scattering angles, each detector bank has a different scaling factor. These scaling factors were estimated by fitting the data collected at 100 K.

$$A_t = A_0 \cos(\omega t + \phi) \exp(-\sigma^2 t^2 / 2) + A_1 [w_1 \exp(-\lambda_1 t) + (1 - w_1) \exp(-\lambda_2 t)] + A_{BG} \quad (4)$$

Here A_0 is the asymmetry associated with the oscillatory component (some time called transverse component), A_1 is the longitudinal component caused by the field component parallel to initial muon spin-polarization and A_{BG} is the background contribution to the asymmetry, representing the muons that missed the sample and stopped in the Ag sample holder. The value of $A_{BG}=0.038$ was

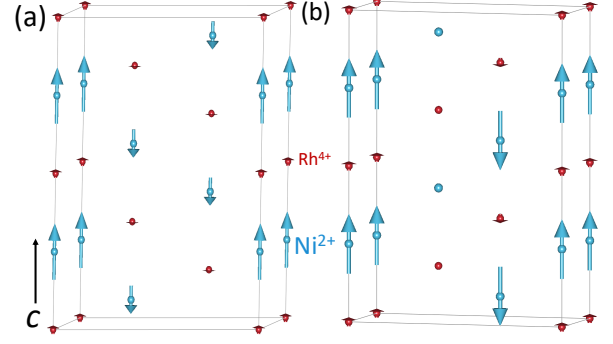


FIG. 4. (Color online) Possible magnetic structures of $\text{Sr}_3\text{NiRhO}_6$ below T_1 (a) Amplitude modulated and (b) PDA structure. Chain with no spin in (b) represent incoherent spin-chain with net zero moment.

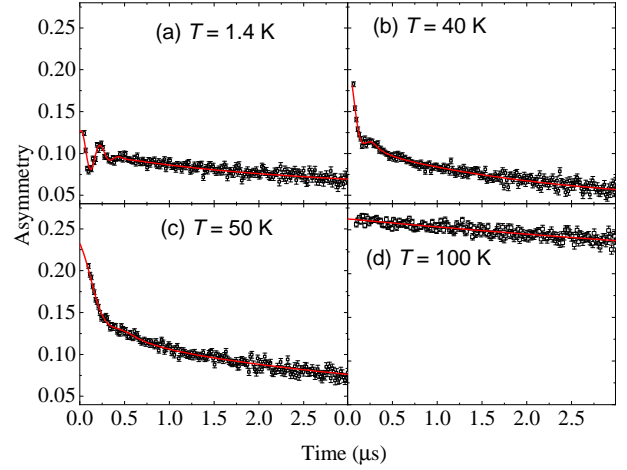


FIG. 5. (Color online) (a-d) ZF- μ SR spectrum of $\text{Sr}_3\text{NiRhO}_6$ at indicated temperatures. The solid curves are the fits to the μ SR data by Eq. 4.

estimated from the fitting of 160 K spectra and was kept fixed during the analysis of other temperature data. Further the value of $w_1 = 0.5$ was kept fixed during the analysis to account the two muon sites, especially in the ordered state. In the paramagnetic state the response from the both the muon stopping sites was assumed identical. Figures 6 (a) and (b) show the T -dependences of the muon precession frequency $f = \omega_{mu}/2\pi$ and its asymmetry A_0 , respectively. The characteristic spin lattice relaxation rates λ_1 and λ_2 are shown in Figure 6 (c). Both f and A_0 have finite value below ~ 50 K, around which a kink has been observed in the dc magnetization study (Fig. 9(b), in the Appendix A) and neutron diffraction (Fig. 3) study shows the presence of long-

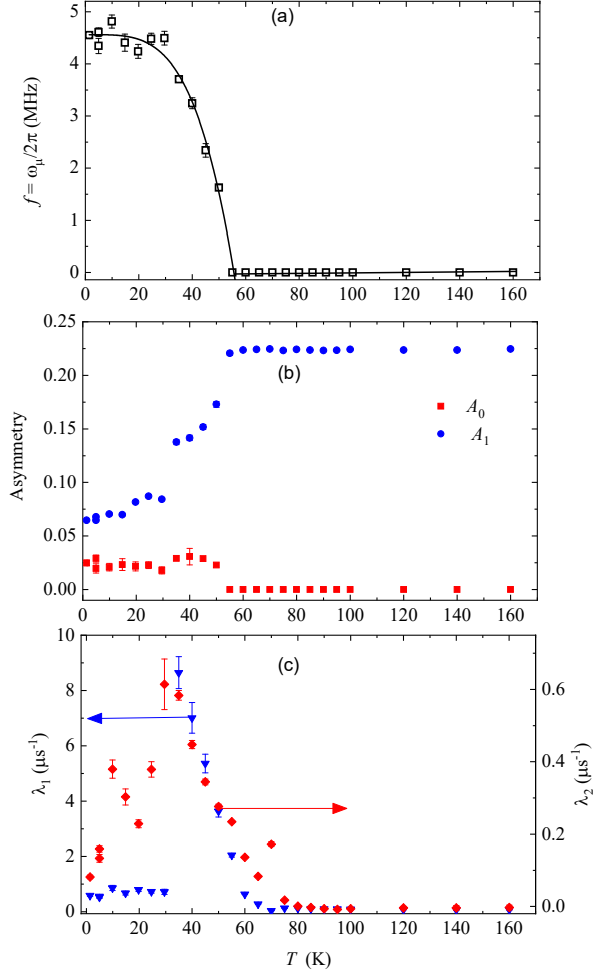


FIG. 6. (Color online) (a) T -dependences of muon precession frequency for $\text{Sr}_3\text{NiRhO}_6$. Solid lines are guide to the eye. (b) T -dependences of a normalized ZF asymmetry. (c) T -dependences of characteristic spin lattice relaxation rates λ_1 and λ_2 .

range magnetic order in PDA state. A change in the spin lattice relaxation rate λ_2 is clearly visible at ~ 20 K, which may be related to the onset of F-PDA state. A simple dipole field calculation shows several frequency components with a large standard deviation are possible for the PDA state. This is consistent with the observed Gaussian damped oscillatory function for the μSR asymmetry spectra.

D. Inelastic Neutron Scattering

To estimate the value of magnetic exchange interactions between localized electron magnetic moments and anisotropy parameters, we have performed INS experiments on $\text{Sr}_3\text{NiRhO}_6$. Figure 7(a)

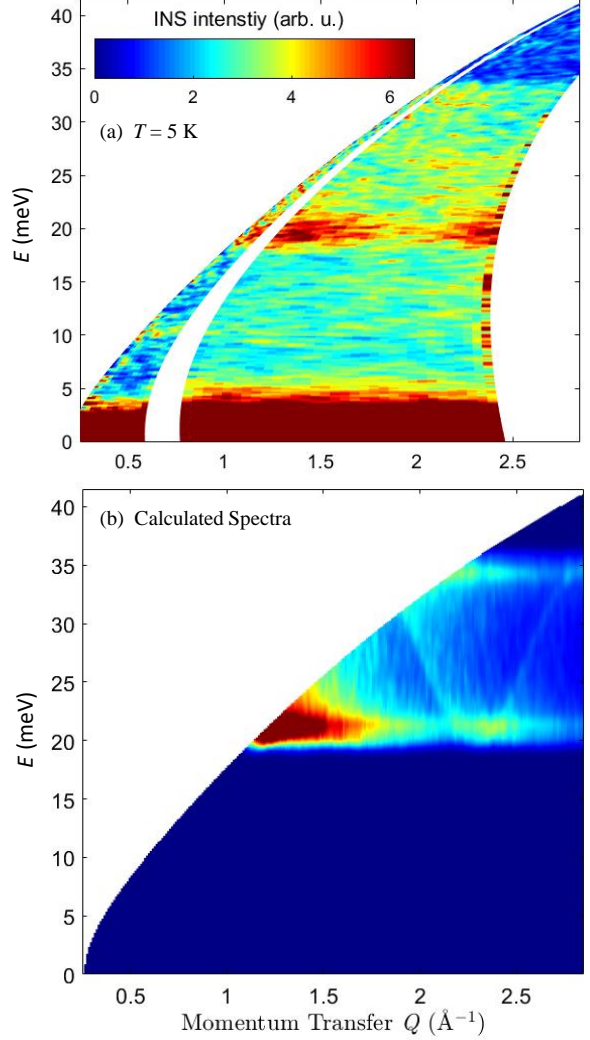


FIG. 7. (Color online) (a) Color coded inelastic neutron scattering intensity maps, energy transfer vs momentum transfer (Q) of $\text{Sr}_3\text{NiRhO}_6$ measured with an incident energy $E_i = 50$ meV on HET. (b) The simulated spin-wave spectra using SpinW program [47] with exchange parameters, $J = 3.7$ meV and a single ion anisotropy $D = 10$ meV for Ni^{2+} spins.

shows the INS response, a color-coded contour map of the intensity, energy transfer E versus momentum transfer Q for $\text{Sr}_3\text{NiRhO}_6$ measured at $T = 5$ K (with $E_i = 50$ meV) from the low-angle detectors banks up to $Q = 3$ \AA^{-1} . The INS spectra show a spin-wave gap of 20 meV and bandwidth of 34 meV. The intensity of the INS signal, energy integrated over 18-23 meV, decreases with increasing value of Q and follows the form factor of Ni^{2+} ($I \propto |f_{\text{Ni}}(Q)|^2$), which is very similar to that observed in $\text{Sr}_3\text{NiIrO}_6$ [38]. This confirms that the magnetic signal arises from Ni^{2+} spin waves. To

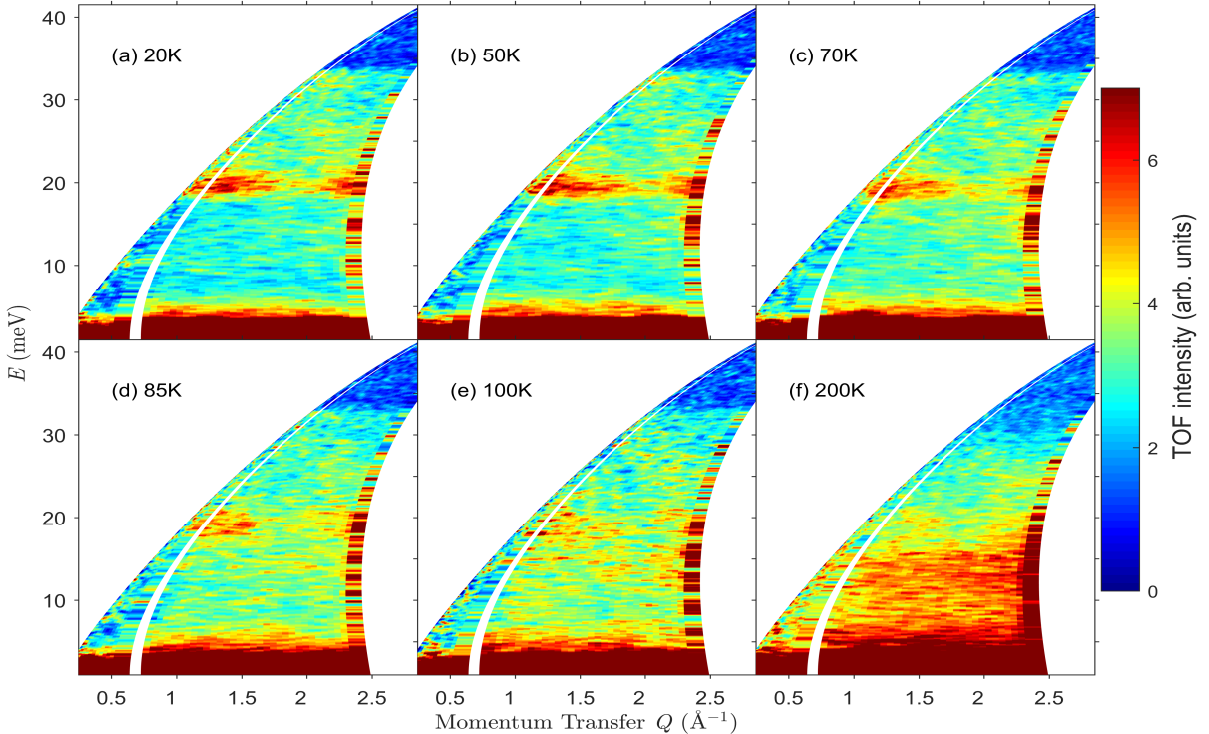


FIG. 8. (Color online) (a-f) Temperature evolution of the INS spectra measured over 20–200 K.

analyze the observed spin wave excitation, we have used the following phenomenological spin Hamiltonian, containing terms only having intra-chain exchange interactions:

$$H = - \sum_i [J \mathbf{S}_i \cdot \mathbf{S}_{i+1} + D S_z^2] \quad (5)$$

Here i is the site index for the Ni^{2+} (TP) ions in the chain, J represents the isotropic Heisenberg coupling between the Ni^{2+} spins, and the z axis is directed along the chains. $D > 0$ is the single-ion anisotropy parameter, and S_z refers to the spin component along the c -axis (chain direction). We have not included interchain interactions in the phenomenological spin Hamiltonian because they are expected to be very weak and thus do not affect the spin-wave dispersion along the chains significantly. In addition, we have not observed any feature associated with Rh^{4+} spin-waves and/or Ni-Rh intra-chain exchange interactions in magnetic excitation spectra, probably due to very small signals and/or these features are present at higher energy as seen for Ir mode near ~ 90 meV in $\text{Sr}_3\text{NiIrO}_6$ [48]. From the observed spectrum, we can set an upper limit of 0.03 meV for the inter-chain AFM interaction. Within the framework of linear spin-wave theory,

the dispersion for the spin Hamiltonian (5) is given by :

$$\hbar\omega_L = 2S[(D + J) - J \cos(\pi L)]. \quad (6)$$

Figure 7(b) shows the powder spectrum simulated by linear spin-wave theory for $J = 3.7$ meV and $D = 10$ meV using spinW [47], which reveals good agreement with the observed spin-wave excitations. The temperature dependence of INS spectra is shown in Fig. 8. Surprisingly, the spin wave excitation survive up to $T = 85$ K (1.5 times T_1), suggesting that intrachain FM correlation builds much above magnetic ordering temperature. Similar behavior has been observed for other compound of $A_3\text{MXO}_6$ family such as $\text{Ca}_3\text{Co}_2\text{O}_6$ [28, 35] and $\text{Sr}_3\text{NiIrO}_6$ [38] (spin-1 and spin-1/2 alternating chain). The observed behavior can be attributed to a quasi-1D nature of the magnetic interactions in $\text{Sr}_3\text{NiRhO}_6$. Upon heating above 85 K, we observe a reduction of the gap and a transfer of spectral weight from higher energy into the spin-gap region.

E. Domain Wall Formation and Dynamics

Having determined the value of exchange and

anisotropy parameters, we now discuss the low energy magnetic excitation in $\text{Sr}_3\text{NiRhO}_6$. From the observed large value of D ($D \gg J$), it is clear that the lowest energy excitation in $\text{Sr}_3\text{NiRhO}_6$, should be a single domain-wall (assuming negligible inter-chain exchange interaction J_{inter}) with energy cost $2JS^2$ (85 K), which can move easily along the chain without any energy cost. The single domain-wall here refers to the two FM regions of opposite polarity. At finite temperature, the total free energy of the system has contribution from entropy ($S = k_B T \log_e N$) also the resulting free energy, therefore, is $F = 2JS^2 - k_B T \log_e N$. An important point to be noted here is that for FM chains, the domain wall can propagate only via a thermally activated process. These thermally activated domain walls lead to high degeneracy in the PDA state at finite temperatures, resulting in more domain wall formation. However, at low temperatures, their propagation becomes extremely slow. Due to this, fluctuating high-temperature multidomains may lead to randomness and disorder at lower temperatures. This results in a transition from PDA to F-PDA-like state, as observed for $\text{Ca}_3\text{CoRhO}_6$ [5, 49]. The observed frequency dependence of real χ'_{ac} and imaginary χ''_{ac} components of ac susceptibility (Appendix A, Figs. 12 and 11) and its persistence under an applied dc magnetic field of ~ 70 kOe, with only a small reduction in its intensity, at ~ 20 K, could be consistently interpreted with the idea of F-PDA-like state.

IV. CONCLUSIONS

In conclusion, we have investigated the magnetic ground state in $\text{Sr}_3\text{NiRhO}_6$ using muon spin rotation and relaxation (μSR), neutron diffraction and inelastic neutron scattering techniques. The neutron diffraction study, combined with ac susceptibility and μSR measurements, indicates the presence of a partially-disordered antiferromagnetic (PDA) state below T_1 . Below T_2 , the 1/3 incoherent spin-chains of PDA structure freeze into a F-PDA-like state (Appendix B). Our INS study showed dispersing magnetic excitations, whose quasi-1D character evidences the prevalence of FM intrachain (anisotropy gap D three times larger than the exchange interaction J) over AFM interchain interactions. The observed large value of D ($D \gg J$) in these triangular lattice antiferromagnets, with FM intrachain interaction, results in the formation of domain walls. Freezing of domain walls results into formation of a F-PDA-like state below T_2 . The present study shows that a F-PDA-like state, as the ground state of the triangular lattice antiferromag-

netic system, presents a complicated spin configuration due to geometrical frustration at low temperatures. The values of exchange parameters obtained in the present study will be helpful to carry out large scale Monte Carlo calculations to estimate the equal time correlation functions and for the development of theoretical models to understand the domain wall dynamics of the PDA state in geometrically frustrated magnets.

ACKNOWLEDGMENTS

D.T.A. thanks the EPSRC UK for funding (Grant No. EP/W00562X/1), the Royal Society of London for International Exchange funding between the UK and Japan, and Newton Advanced Fellowship funding between the UK and China and the CAS for PIFI Fellowship. SMY acknowledges the financial assistance from SERB, Department of Science and Technology, Government of India under the J C Bose fellowship program (JCB/2023/000014).

Appendix A: Dc Magnetization

Figure 9 shows the dc magnetization measurements for $\text{Sr}_3\text{NiRhO}_6$ under various applied magnetic field of 1, 25, 10, and 70 kOe. Under zero field cooled (ZFC) condition [Fig 9(a)], magnetization increases gradually with decreasing the temperature. A kink is observed in the ZFC magnetization at ~ 50 K (T_1), indicating the onset of a magnetic phase transition [(Fig 9(b))]. Both field cooled (FC) and ZFC magnetizations increase sharply below T_1 . At low temperature ~ 15 K (T_2), a sharp drop in the ZFC magnetization along with a bifurcation in the FC and ZFC magnetization has been observed, which could be due to (i) a possible spin freezing due to the presence of competing exchange interactions and (ii) domain wall freezing. In addition, at ~ 10 K, a small kink has also been observed in the magnetization curves. Similar two characteristic temperatures T_1 and T_2 have been reported in literature for the other compounds of the A_3MXO_6 family, such as $\text{Ca}_3\text{CoRhO}_6$ [8, 49, 50], and $\text{Sr}_3\text{NiIrO}_6$ [9, 27]. For both compounds, neutron diffraction studies have confirmed a partially disordered antiferromagnetic (PDA) state or amplitude modulated structure [in latter case [34]].

High temperature inverse magnetic susceptibility (χ^{-1}), shown in Fig 9(c), follows Curie-Weiss law with a paramagnetic Curie temperature (θ_{CW}) of 16.2 K. The derived value of the effective moment

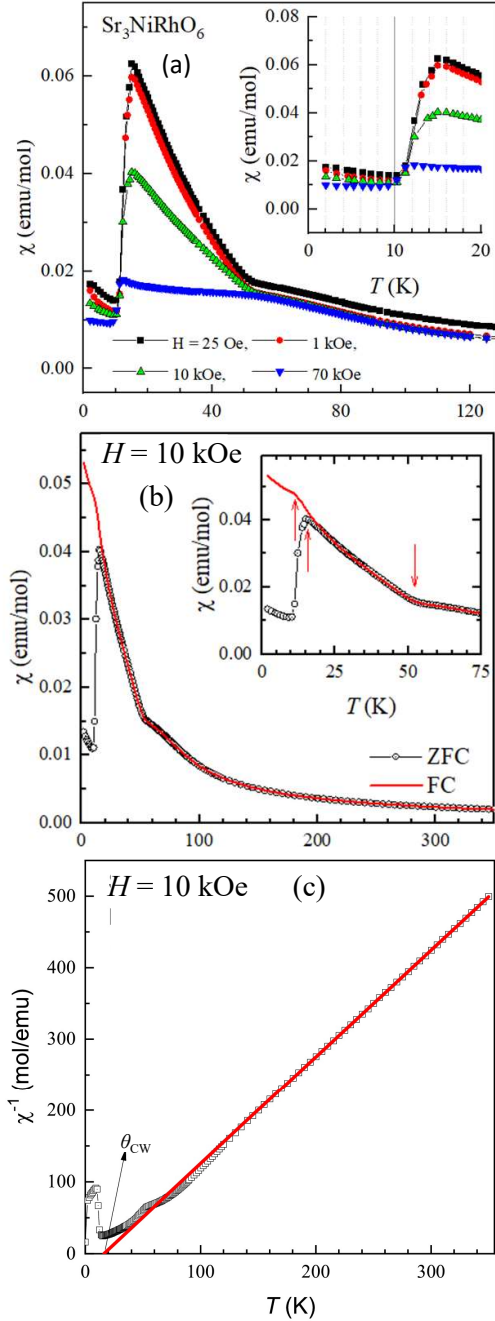


FIG. 9. (Color online) (a) Temperature variation of the dc magnetization under various applied magnetic field for $\text{Sr}_3\text{NiRhO}_6$. (b) Temperature dependence of the field cooled (FC) and zero field cooled (ZFC) magnetization for $\text{Sr}_3\text{NiRhO}_6$ under applied magnetic field of 10 kOe. (c) Temperature variation of high temperature inverse magnetic susceptibility under applied magnetic field of 10 kOe.

from the slope of the fitting results in $2.3 \mu_B/\text{f.u.}$. The observed value of the effective paramagnetic moment is less than the theoretically expected value of $3.2 \mu_B/\text{f.u.}$, considering $S = 1/2$ and 1 for Rh^{4+} and Ni^{2+} , respectively (with $g = 2$). The observed small value of the magnetic moment could be due to strong covalent mixing, expected in $4d$ transition metal oxides. Since θ_{CW} represent the combined effect of all exchange interactions, the observed positive value indicates that dominant exchange interaction in $\text{Sr}_3\text{NiRhO}_6$ is FM.

To understand the magnetization behavior in $\text{Sr}_3\text{NiRhO}_6$, we have measured dc magnetization as function of applied magnetic field at various temperatures over 1.5-60 K (Fig. 10). A paramagnetic-like behavior has been observed above T_1 (50 K). Below T_1 , a curvature has been observed in the magnetization curves, which becomes prominent below 40 K. For $10.5 \leq T \leq 20$ K, a step like shape of the magnetization is clearly visible. The value of the magnetization in the plateau region is $\sim 0.2 \mu_B$, which is close to 1/3 of the expected value of the full ordered moment (obtained from neutron diffraction study discussed in the main text) considering a fully polarized FM state, with parallel alignment of all Rh^{4+} and Ni^{2+} spins in a unit cell. The observed step-like behavior could be due to a magnetic field induced transition to a ferrimagnetic state, where two thirds of the spin-chains have spin up and the remaining one third have spin down. For $8.25 \leq T \leq 11$ K, the revised leg of the $M(H)$ curve, while approaching a zero field, shows that hysteresis is present. The observed hysteresis occupies all field range for $8.2 < T < 10.5$ K, however, it is very weak for $2 \leq T \leq 7.5$ K, with no saturation of the magnetization under highest applied magnetic field of 7 T.

Appendix B: Ac Susceptibility

To probe the origin of the bifurcation in the FC and ZFC magnetization and get a better insight of the magnetic dynamics in $\text{Sr}_3\text{NiRhO}_6$, we have measured ac susceptibility as a function of temperature at various frequencies. A peak in the ac susceptibility has been observed (Fig. 11) at ~ 20 K in both real and imaginary part of the ac susceptibility. Peak shifts to the higher temperature by increasing the frequency of the applied ac field indicated the onset of glassiness around 20 K. Surprisingly, the observed shift in the position of the ac susceptibility peak is much larger than expected for a conventional spin-glass system. It may be remarked that under applied dc magnetic field of 70 kOe, the peak in both

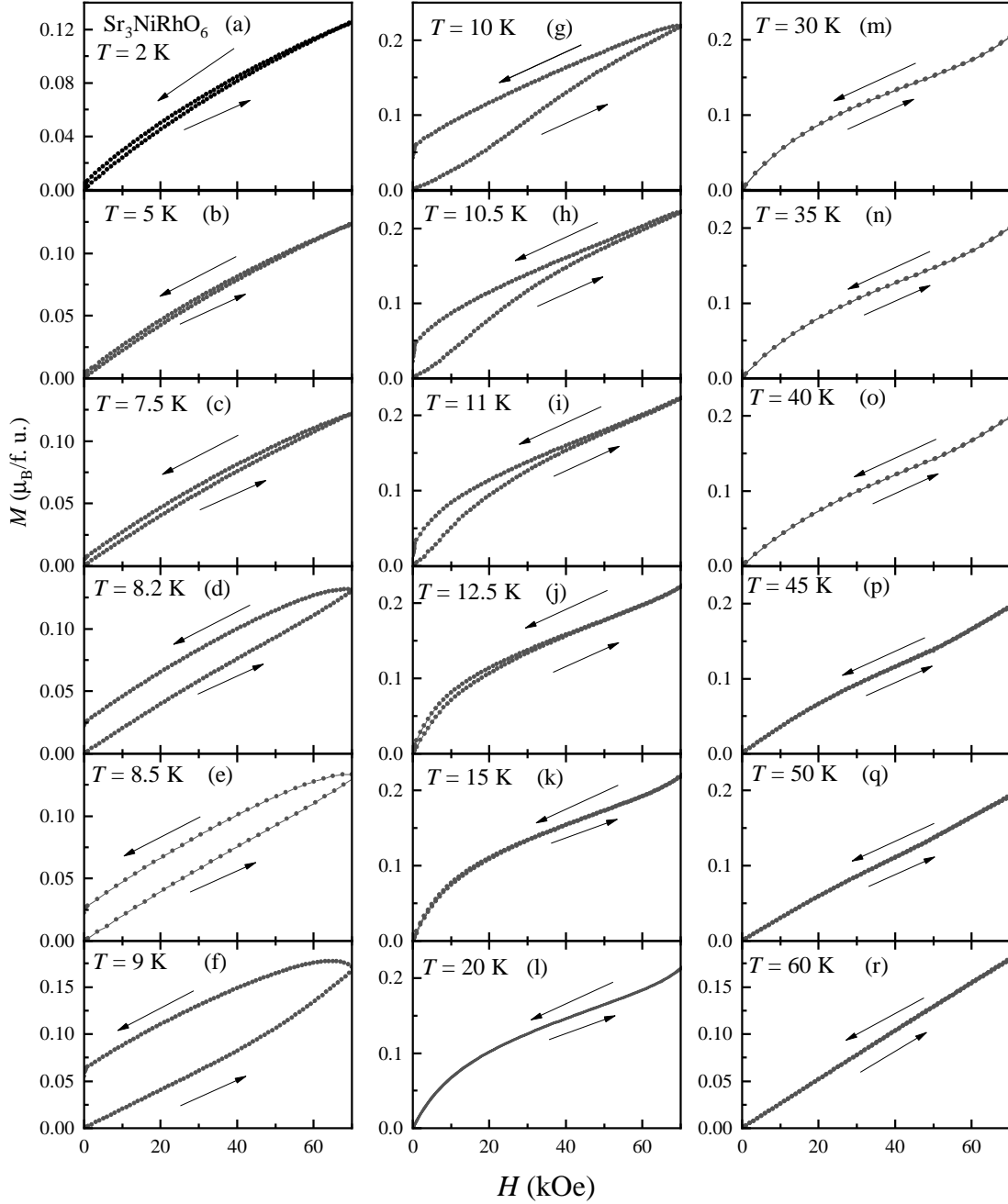


FIG. 10. (Color online) Isothermal dc magnetization for $\text{Sr}_3\text{NiRhO}_6$ at various temperatures. The arrows indicate direction of external magnetic field variation.

χ'_{ac} and χ''_{ac} persists, with only a small reduction in its intensity. These observations reveal that the χ'_{ac} signal in zero field is made up of a FM part and a spin-glass part. Under applied dc magnetic field of 70 kOe, the spin-glass part gets suppressed, however, the FM part behave like clusters (created by negligible motion of domain wall) with some glassy

dynamics.

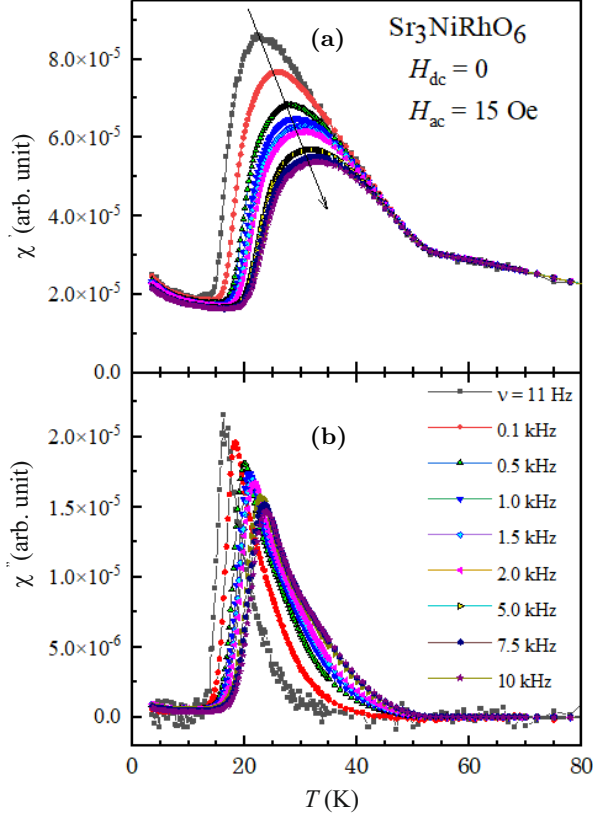


FIG. 11. (Color online) The temperature dependence of (a) real and (b) imaginary parts of ac susceptibility for $\text{Sr}_3\text{NiRhO}_6$ at varied frequencies under zero applied dc magnetic field.

Appendix C: Additional Neutron Diffraction Patterns

A neutron diffraction pattern has been recorded over wide Q -range (Fig. 13) using GEM TOF diffractometer at ISIS Facility, to examine if there is any anti-site mixing for Ni/Rh. The analysis has revealed no improvement of the fit when varying the occupancies of both Ni and Rh from their expected values. This rules out the possibility of anti-site mixing in our sample.

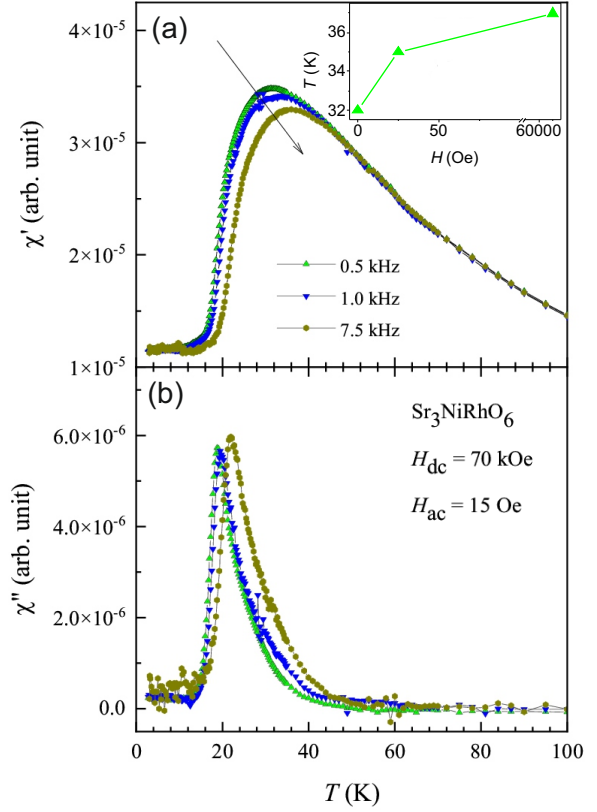


FIG. 12. (Color online) The temperature dependence of (a) real and (b) imaginary parts of ac susceptibility for $\text{Sr}_3\text{NiRhO}_6$ at varied frequencies under dc magnetic field of 70 kOe. Inset in (a) shows field variations of the center of the peak observed in χ'_{ac} .

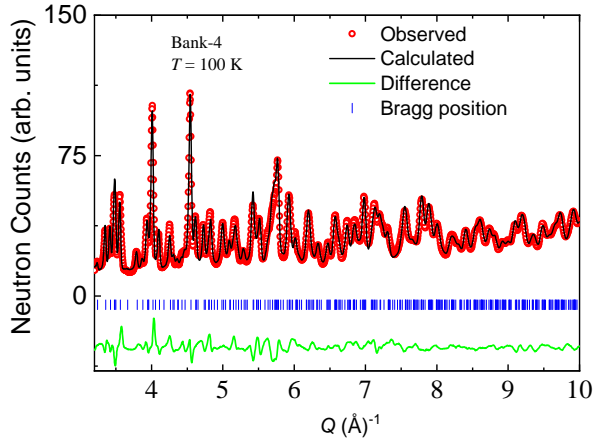


FIG. 13. (Color online) Observed (open circles) and calculated (solid lines) neutron diffraction patterns at 100 K for $\text{Sr}_3\text{NiRhO}_6$ over high values of Q from the GEM TOF diffractometer. The green solid line at the bottom shows the difference between the observed and the calculated patterns. Vertical lines show the positions of the nuclear Bragg peaks.

- * ajain@barc.gov.in
† devashibhai.adroja@stfc.ac.uk
- [1] N. Mohapatra, K. K. Iyer, S. Rayaprol, and E. V. Sampathkumaran, Geometrically frustrated magnetic Behavior of $\text{Sr}_3\text{NiRhO}_6$ and $\text{Sr}_3\text{NiPtO}_6$, *Phys. Rev. B* **75**, 214422 (2007).
 - [2] T. Nguyen and H.-C. zur Loye, A Family of One-Dimensional Oxides: Sr_3MlrO_6 ($M = \text{Ni, Cu, Zn}$): Structure and Magnetic Properties, *J. Solid State Chem.* **117**, 300 (1995).
 - [3] S. Aasland, H. Fjellvåg, and B. Hauback, Magnetic properties of the one-dimensional $\text{Ca}_3\text{Co}_2\text{O}_6$, *Solid State Communications* **101**, 187 (1997).
 - [4] A. Niazi, E. V. Sampathkumaran, P. L. Paulose, D. Eckert, A. Handstein, and K. H. Müller, $\text{Sr}_3\text{CuIrO}_6$, a spin-chain compound with random ferromagnetic-antiferromagnetic interactions, *Solid State Communications* **120**, 11 (2001).
 - [5] E. V. Sampathkumaran and A. Niazi, Superparamagnetic-like ac susceptibility behavior in the partially disordered antiferromagnetic compound $\text{Ca}_3\text{CoRhO}_6$, *Phys. Rev. B* **65**, 180401(R) (2002).
 - [6] A. Niazi, P. L. Paulose, and E. V. Sampathkumaran, Inhomogeneous Magnetism in Single Crystalline $\text{Sr}_3\text{CuIrO}_{6+\delta}$: Implications to Phase Separation Concepts, *Physical review letters* **88**, 107202 (2002).
 - [7] A. Niazi, E. V. Sampathkumaran, P. L. Paulose, D. Eckert, A. Handstein, and K. H. Müller, Magnetic anomalies in the spin-chain system $\text{Sr}_3\text{Cu}_{1-x}\text{Zn}_x\text{IrO}_6$, *Phys. Rev. B* **65**, 064418 (2002).
 - [8] M. Loewenhaupt, W. Schaefer, A. Niazi, and E. V. Sampathkumaran, Evidence for the coexistence of low-dimensional magnetism and long-range order in $\text{Ca}_3\text{CoRhO}_6$, *Europhysics Letters* **63**, 374 (2003).
 - [9] D. Flahaut, S. Hebert, A. Maignan, V. Hardy, C. Martin, M. Hervieu, M. Costes, B. Raquet, and J. M. Broto, A magnetic study of the one dimensional $\text{Sr}_3\text{NiIrO}_6$ compound, *Eur. Phys. J. B* **35**, 317 (2003).
 - [10] S. Rayaprol, K. Sengupta, and E. Sampathkumaran, Magnetic behaviour of quasi-one-dimensional oxides, $\text{Ca}_3\text{Co}_{1+x}\text{Mn}_{1-x}\text{O}_6$, *Solid State Communications* **128**, 79 (2003).
 - [11] E. V. Sampathkumaran, N. Fujiwara, S. Rayaprol, P. K. Madhu, and Y. Uwatoko, Magnetic behavior of Co ions in the exotic spin-chain compound $\text{Ca}_3\text{Co}_2\text{O}_6$ from ^{59}Co NMR studies, *Physical Review B - Condensed Matter and Materials Physics* **70**, 014437 (2004).
 - [12] E. V. Sampathkumaran, Z. Hiroi, S. Rayaprol, and Y. Uwatoko, Heat-capacity anomalies in the presence of high magnetic fields in the spin-chain compound, $\text{Ca}_3\text{Co}_2\text{O}_6$, *J. Magn. Magn. Mater.* **284**, L7 (2004).
 - [13] V. Hardy, M. R. Lees, O. A. Petrenko, D. M. Paul, D. Flahaut, S. Hébert, and A. Maignan, Temperature and time dependence of the field-driven magnetization steps in $\text{Ca}_3\text{Co}_2\text{O}_8$ single crystals, *Phys. Rev. B* **70**, 064424 (2004).
 - [14] K. Takubo, T. Mizokawa, S. Hirata, J. Y. Son, A. Fujimori, D. Topwal, D. D. Sarma, S. Rayaprol, and E. V. Sampathkumaran, Electronic structure of Ca_3CoXO_6 ($X=\text{Co, Rh, Ir}$) studied by x-ray photoemission spectroscopy, *Physical Review B - Condensed Matter and Materials Physics* **71**, 073406 (2005).
 - [15] H. Wu, M. W. Haverkort, Z. Hu, D. I. Khomskii, and L. H. Tjeng, Nature of magnetism in $\text{Ca}_3\text{Co}_2\text{O}_6$, *Phys. Rev. Lett.* **95**, 186401 (2005).
 - [16] A. Jain, S. Singh, and S. M. Yusuf, Structural and magnetic properties of spin chain compounds $\text{Ca}_3\text{Co}_{2-x}\text{Fe}_x\text{O}_6$, *Phys. Rev. B* **74**, 174419 (2006).
 - [17] E. V. Sampathkumaran, N. Mohapatra, S. Rayaprol, and K. K. Iyer, Magnetic anomalies in a spin-chain compound, $\text{Sr}_3\text{CuRhO}_6$: Griffiths-phase-like behavior of magnetic susceptibility, *Phys. Rev. B* **75**, 052412 (2007).
 - [18] S. Agrestini, L. C. Chapon, A. Daoud-Aladine, J. Schefer, A. Gukasov, C. Mazzoli, M. R. Lees, and O. A. Petrenko, Nature of the magnetic order in $\text{Ca}_3\text{Co}_2\text{O}_6$, *Phys. Rev. Lett.* **101**, 097207 (2008).
 - [19] Y. J. Choi, H. T. Yi, S. Lee, Q. Huang, V. Kiryukhin, and S.-W. Cheong, Ferroelectricity in an Ising Chain Magnet, *Phys. Rev. Lett.* **100**, 047601 (2008).
 - [20] L. C. Chapon, Origin of the long-wavelength magnetic modulation in $\text{Ca}_3\text{Co}_2\text{O}_6$, *Phys. Rev. B* **80**, 172405 (2009).
 - [21] V. Kiryukhin, S. Lee, W. Ratcliff, Q. Huang, H. T. Yi, Y. J. Choi, and S.-W. Cheong, Order by Static Disorder in the Ising Chain Magnet $\text{Ca}_3\text{Co}_{2-x}\text{Mn}_x\text{O}_6$, *Phys. Rev. Lett.* **102**, 187202 (2009).
 - [22] S. Sarkar, S. Kanungo, and T. Saha-Dasgupta, Ab initio study of low-dimensional quantum spin systems Sr_3NiPO_6 , $\text{Sr}_3\text{CuPtO}_6$, and $\text{Sr}_3\text{NiIrO}_6$, *Phys. Rev. B* **82**, 235122 (2010).
 - [23] A. D. Hillier, D. T. Adroja, W. Kockelmann, L. C. Chapon, S. Rayaprol, P. Manuel, H. Michor, and E. V. Sampathkumaran, Noncollinear magnetic order in the $S = \frac{1}{2}$ magnet $\text{Sr}_3\text{ZnRhO}_6$, *Phys. Rev. B* **83**, 024414 (2011).
 - [24] S. Agrestini, C. L. Fleck, L. C. Chapon, C. Mazzoli, A. Bombardi, M. R. Lees, and O. A. Petrenko, Slow Magnetic Order-Order Transition in the Spin Chain Antiferromagnet $\text{Ca}_3\text{Co}_2\text{O}_6$, *Phys. Rev. Lett.* **106**, 197204 (2011).
 - [25] A. Jain and S. M. Yusuf, Short-range and long-range incommensurate magnetic ordering in the frustrated antiferromagnets $\text{Ca}_3\text{Co}_{2-x}\text{Fe}_x\text{O}_6$: A neutron diffraction study, *Phys. Rev. B* **83**, 184425 (2011).
 - [26] T. Moyoshi and K. Motoya, Incommensurate Magnetic Structure and Its Long-Time Variation in a Geometrically Frustrated Magnet $\text{Ca}_3\text{Co}_2\text{O}_6$, *J. Phys. Soc. Jpn.* **80**, 034701 (2011).

- [27] D. Mikhailova, B. Schwarz, A. Senyshyn, A. M. T. Bell, Y. Skourski, H. Ehrenberg, A. A. Tsirlin, S. Agrestini, M. Rotter, P. Reichel, J. M. Chen, Z. Hu, Z. M. Li, Z. F. Li, and L. H. Tjeng, Magnetic properties and crystal structure of $\text{Sr}_3\text{CoIrO}_6$ and $\text{Sr}_3\text{NiIrO}_6$, *Phys. Rev. B* **86**, 134409 (2012).
- [28] A. Jain, P. Y. Portnichenko, H. Jang, G. Jackeli, G. Friemel, A. Ivanov, A. Piovano, S. M. Yusuf, B. Keimer, and D. S. Inosov, One-dimensional dispersive magnon excitation in the frustrated spin-2 chain system $\text{Ca}_3\text{Co}_2\text{O}_6$, *Phys. Rev. B* **88**, 224403 (2013).
- [29] T. Basu, K. K. Iyer, K. Singh, and E. V. Sampathkumaran, Novel dielectric anomalies due to spin-chains above and below Néel temperature in $\text{Ca}_3\text{Co}_2\text{O}_6$, *Scientific reports* **3**, 3104 (2013).
- [30] W. G. Yin, X. Liu, A. M. Tsvelik, M. P. M. Dean, M. H. Upton, J. Kim, D. Casa, A. Said, T. Gog, T. F. Qi, G. Cao, and J. P. Hill, Ferromagnetic exchange anisotropy from antiferromagnetic superexchange in the mixed $3d - 5d$ transition-metal compound $\text{Sr}_3\text{CuIrO}_6$, *Phys. Rev. Lett.* **111**, 057202 (2013).
- [31] S. M. Yusuf, A. Jain, and L. Keller, Field induced incommensurate-to-commensurate magnetic phase transition in $\text{Ca}_3\text{Co}_{1.8}\text{Fe}_{0.2}\text{O}_6$: a neutron diffraction study, *J. Phys.: Condens. Matter* **25**, 146001 (2013).
- [32] A. Jain, S. M. Yusuf, S. S. Meena, and C. Ritter, Stabilization of the spin density wave structure with rare-earth substitution in $\text{Ca}_3\text{Co}_2\text{O}_6$, *Phys. Rev. B* **87**, 094411 (2013).
- [33] X. Ou and H. Wu, Impact of spin-orbit coupling on the magnetism of $\text{Sr}_3\text{M}(\text{IrO}_6)$ ($M = \text{Ni}, \text{Co}$), *Scientific reports* **4**, 4609 (2014).
- [34] E. Lefrançois, L. C. Chapon, V. Simonet, P. Lejay, D. Khalyavin, S. Rayaprol, E. V. Sampathkumaran, R. Ballou, and D. T. Adroja, Magnetic order in the frustrated ising-like chain compound $\text{Sr}_3\text{NiIrO}_6$, *Physical Review B* **90**, 014408 (2014).
- [35] S. Agrestini, D. T. Adroja, M. Rotter, S. Majumdar, M. R. Lees, B. G., D. Paul, and Y. Y. Yeung, No title, unpublished (2014).
- [36] T. Basu, K. Iyer, K. Singh, K. Mukherjee, P. Paulose, and E. Sampathkumaran, Anisotropic magnetodielectric coupling behavior of $\text{Ca}_3\text{Co}_{1.4}\text{Rh}_{0.6}\text{O}_6$ due to geometrically frustrated magnetism, *Appl. Phys. Lett.* **105**, 102912 (2014).
- [37] J. A. M. Paddison, S. Agrestini, M. R. Lees, C. L. Fleck, P. P. Deen, A. L. Goodwin, J. R. Stewart, and O. A. Petrenko, Spin correlations in $\text{Ca}_3\text{Co}_2\text{O}_6$: Polarized-neutron diffraction and monte carlo study, *Phys. Rev. B* **90**, 014411 (2014).
- [38] S. Toth, W. Wu, D. T. Adroja, S. Rayaprol, and E. V. Sampathkumaran, Frustrated Ising chains on the triangular lattice in $\text{Sr}_3\text{NiIrO}_6$, *Phys. Rev. B* **93**, 174422 (2016).
- [39] P. A. McClarty, A. D. Hillier, D. T. Adroja, D. D., S. Rayaprol, P. Manuel, W. Kockelmann, and E. V. Sampathkumaran, Non-collinear Order and Spin-Orbit Coupling in $\text{Sr}_3\text{ZnIrO}_6$, *Journal of the Physical Society of Japan* **89**, 064703 (2020).
- [40] S. M. Yusuf, A. Jain, A. K. Bera, S. S. Meena, D. K. Shukla, and J. Stempffer, Time and magnetic field dependent magnetic order in $\text{Ca}_3\text{Co}_2\text{O}_6$ revealed by resonant x-ray scattering, *Phys. Rev. B* **107**, 184406 (2023).
- [41] B. J. Kim, H. Ohsumi, T. Komesu, S. Sakai, T. Morita, H. Takagi, and T. Arima, Phase-Sensitive Observation of a Spin-Orbital Mott State in Sr_2IrO_4 , *Science* **323**, 1329 (1948).
- [42] T. Birol, K. Haule, and D. Vanderbilt, Nature of the magnetic interactions in $\text{Sr}_3\text{NiIrO}_6$, *Phys. Rev. B* **98**, 134432 (2018).
- [43] J. Rodríguez-carvajal, Recent advances in magnetic structure determination by neutron powder diffraction, *Physica B: Condensed Matter* **192**, 55 (1993).
- [44] K. Stitzer, W. Henley, J. Claridge, H.-C. zur Loye, and R. Layland, $\text{Sr}_3\text{NiRhO}_6$ and $\text{Sr}_3\text{CuRhO}_6$ —Two New One-Dimensional Oxides. Magnetic Behavior as a Function of Structure: Commensurate vs Incommensurate, *Journal of Solid State Chemistry* **164**, 220 (2002).
- [45] G. V. Vajenine, R. Hoffmann, and H. C. Zur Loye, The electronic structures and magnetic properties of one-dimensional ABO_6 chains in Sr_3ABO_6 ($A = \text{Co}, \text{Ni}$; $B = \text{Pt}, \text{Ir}$) and two-dimensional MO_3 sheets in InMO_3 ($M = \text{Fe}, \text{Mn}$), *Chemical Physics* **204**, 469 (1996).
- [46] E. F. Bertaut, Spin configurations in ionic structures: Theory and practice in magnetism, edited by g.t. rado and h. suhl, in *Magnetism*, Vol. III, edited by G. T. Rado and H. Suhl (Academic Press, New York, 1965) p. 105.
- [47] S. Toth and B. Lake, Linear spin wave theory for single-Q incommensurate magnetic structures, *J. Phys.: Condens. Matter* **27**, 166002 (2015).
- [48] E. Lefrançois, A.-M. Pradipto, M. Moretti Sala, L. C. Chapon, V. Simonet, S. Picozzi, P. Lejay, S. Petit, and R. Ballou, Anisotropic interactions opposing magnetocrystalline anisotropy in $\text{Sr}_3\text{NiIrO}_6$, *Phys. Rev. B* **93**, 224401 (2016).
- [49] S. Niitaka, K. Yoshimura, K. Kosuge, M. Nishi, and K. Kakurai, Partially Disordered Antiferromagnetic Phase in $\text{Ca}_3\text{CoRhO}_6$, *Phys. Rev. Lett.* **87**, 177202 (2001).
- [50] S. Niitaka, H. Kageyama, K. Yoshimura, K. Kosuge, S. Kawano, N. Aso, A. Mitsuda, H. Mitamura, and T. Goto, High-field magnetization and neutron diffraction studies of one-dimensional compound $\text{Ca}_3\text{CoRhO}_6$, *Jpn. J. Appl. Phys.* **70**, 1222 (2001).